### Title
Non-Invasive In Vivo Characterization of Breast Tumors Using Photon Migration Spectroscopy




### Journal
Neoplasia (New York, N.Y.), 2(1-2)

### ISSN
1476-5586



### Authors
Tromberg, Bruce J
Shah, Natasha
Lanning, Ryan
et al.



### Publication Date
2000

Peer reviewed

Neoplasia • Vol. 2, Nos. 1–2, January-April 2000, pp. 26–40 **26**

www.nature.com/neo

# Non-Invasive *In Vivo* Characterization of Breast Tumors Using Photon Migration Spectroscopy[1]

*Bruce J. Tromberg*, Natasha Shah*, Ryan Lanning*, Albert Cerussi*, Jennifer Espinoza*, Tuan Pham*, Lars Svaasand[†] and John Butler[‡]*

*Laser Microbeam and Medical Program (LAMMP), Beckman Laser Institute and Medical Clinic, University of California, Irvine, CA; [†]NTNU, Norwegian Technological University, Trondheim, Norway; [‡]Department of Surgery, University of California, Irvine, CA

**Abstract**

**Frequency-domain photon migration (FDPM) is a non-invasive optical technique that utilizes intensity-modulated, near-infrared (NIR) light to quantitatively measure optical properties in thick tissues. Optical properties (absorption, $\mu_a$, and scattering, $\mu_s'$, parameters) derived from FDPM measurements can be used to construct low-resolution (0.5 to 1 cm) functional images of tissue hemoglobin (total, oxy-, and deoxy-forms), oxygen saturation, blood volume fraction, water content, fat content and cellular structure. Unlike conventional NIR transillumination, FDPM enables quantitative analysis of tissue absorption and scattering parameters in a single non-invasive measurement. The unique functional information provided by FDPM makes it well-suited to characterizing tumors in thick tissues. In order to test the sensitivity of FDPM for cancer diagnosis, we have initiated clinical studies to quantitatively determine normal and malignant breast tissue optical and physiological properties in human subjects. Measurements are performed using a non-invasive, multi-wavelength, diode-laser FDPM device optimized for clinical studies. Results show that ductal carcinomas (invasive and *in situ*) and benign fibroadenomas exhibit 1.25 to 3-fold higher absorption than normal breast tissue. Within this group, absorption is greatest for measurements obtained from sites of invasive cancer. Optical scattering is approximately 20% greater in pre-menopausal versus post-menopausal subjects due to differences in gland/cell proliferation and collagen/fat content. Spatial variations in tissue scattering reveal the loss of differentiation associated with breast disease progression. Overall, the metabolic demands of hormonal stimulation and tumor growth are detectable using photon migration techniques. Measurements provide quantitative optical property values that reflect changes in tissue perfusion, oxygen consumption, and cell/matrix development.** *Neoplasia* (2000) **2,** 26–40.

**Keywords:** tissue optical properties, absorption, scattering, diffuse optical imaging, near-infrared spectroscopy, hemoglobin, tumor vasculature, extracellular matrix.

## Introduction

Pathologists routinely examine thin sections of surgically removed tissue in order to diagnose cancer. If similar information could be provided by techniques that allow us to see internal structure, physicians would be able to find and characterize tumors non-invasively. Historically, this reasoning lead to the development of "diaphanography", a near-infrared (NIR) light imaging method introduced nearly 70 years ago to locate and identify breast cancer [1]. NIR imaging is a simple, low-cost, risk-free procedure that, unlike X-ray mammography, does not employ ionizing radiation. Unfortunately, the initial promise of NIR diaphanography was never realized, primarily due to intense light scattering.

Distinguishing between absorption and scattering is generally recognized as one of the principal limitations to detecting cancer with light. This problem has challenged scientists who study how light interacts with turbid materials for many years. Recent developments in theory and instrumentation, collectively referred to as "photon migration" (PM), now enable us to probe and analyze multiply-scattered light signals on an ultra-fast time scale (e.g., picoseconds). These technological advances provide a simple framework for measuring the exact magnitude of absorption and scattering (i.e., optical properties) in turbid materials. Optical properties can, in turn, be used to locate and identify physiological changes characteristic of tumors, hormonal stimulation, pharmacologic agents, and age-related tissue remodeling.

Research by our group and many others in the Biomedical Optics community has helped rejuvenate interest in optical methods for detecting and characterizing solid tumors [2]. The use of ultra-fast light provides new information with the

Address all correspondence to: Dr. Bruce J. Tromberg, Laser Microbeam and Medical Program, Beckman Laser Institute and Medical Clinic, 1002 Health Sciences Road, East, University of California, Irvine, CA 92612-1475. E-mail: tromberg@bli.uci.edu

[1]This work was made possible, in part, through access to the Laser Microbeam and Medical Program (LAMMP) and the Chao Family Cancer Center at the University of California, Irvine. These facilities are supported by the National Institutes of Health under grants RR-01192 and CA-62203, respectively. Support was also provided by the NIH Institute of General Medical Sciences (GM-50958), the Department of Energy (DOE #DE-FG03-91ER61227), the U.S. Army Breast Cancer Research Program, and the Beckman Foundation.

Received 14 December 1999; Accepted 20 December 1999.

same advantages as conventional NIR diaphanography (e.g., low cost, zero risk, compact devices). However, in order to demonstrate whether normal and malignant structures can actually be resolved using light, reliable measurements of both normal and tumor tissue optical properties must be performed in human subjects.

Few studies have been completed that accurately measure human tissue optical properties *in vivo*. This can be a particularly difficult hurdle to overcome because photon migration, as a fundamentally new method, is not widely accessible. PM technology development requires interdisciplinary expertise in diverse fields while measurements require strong clinical collaborations. Clinical studies are now underway here (about 70 human subjects have been enrolled in breast, brain, and cervical protocols to date) and in other laboratories that will provide critical information for determining whether non-invasive photon migration measurements are useful for characterizing, imaging, and detecting solid tumors. Early results show that unique tumor optical signatures are, in fact, measurable. Organs of greatest initial promise appear to be breast and brain. Changes in blood flow, oxygen consumption, and tissue architecture (cellular and matrix) can be measured in these structures quantitatively using NIR photon migration. Most importantly, these signals appear to reflect fundamental physiological processes associated with malignancy, disease progression, and response to therapy.

In this work, we review basic principles of photon migration [3] in thick tissues and highlight how light–tissue interaction mechanisms provide unique opportunities for solid tumor diagnostics. Details of instrumentation and theory development in photon migration spectroscopy are presented along with results of clinical studies in human breast tumor patients. Because many attributes related to the origin, progression, and therapeutic response of breast cancers are common to other types of tumors, these data should provide insight into how continued optical technology development will impact cancer diagnosis and screening.

## Light Propagation in Thick Tissues

### *Spectral Dependence*

Light propagation in biological tissues is a complex function of scattering and absorption, which, in turn, are dependent on cellular structure and molecular composition.

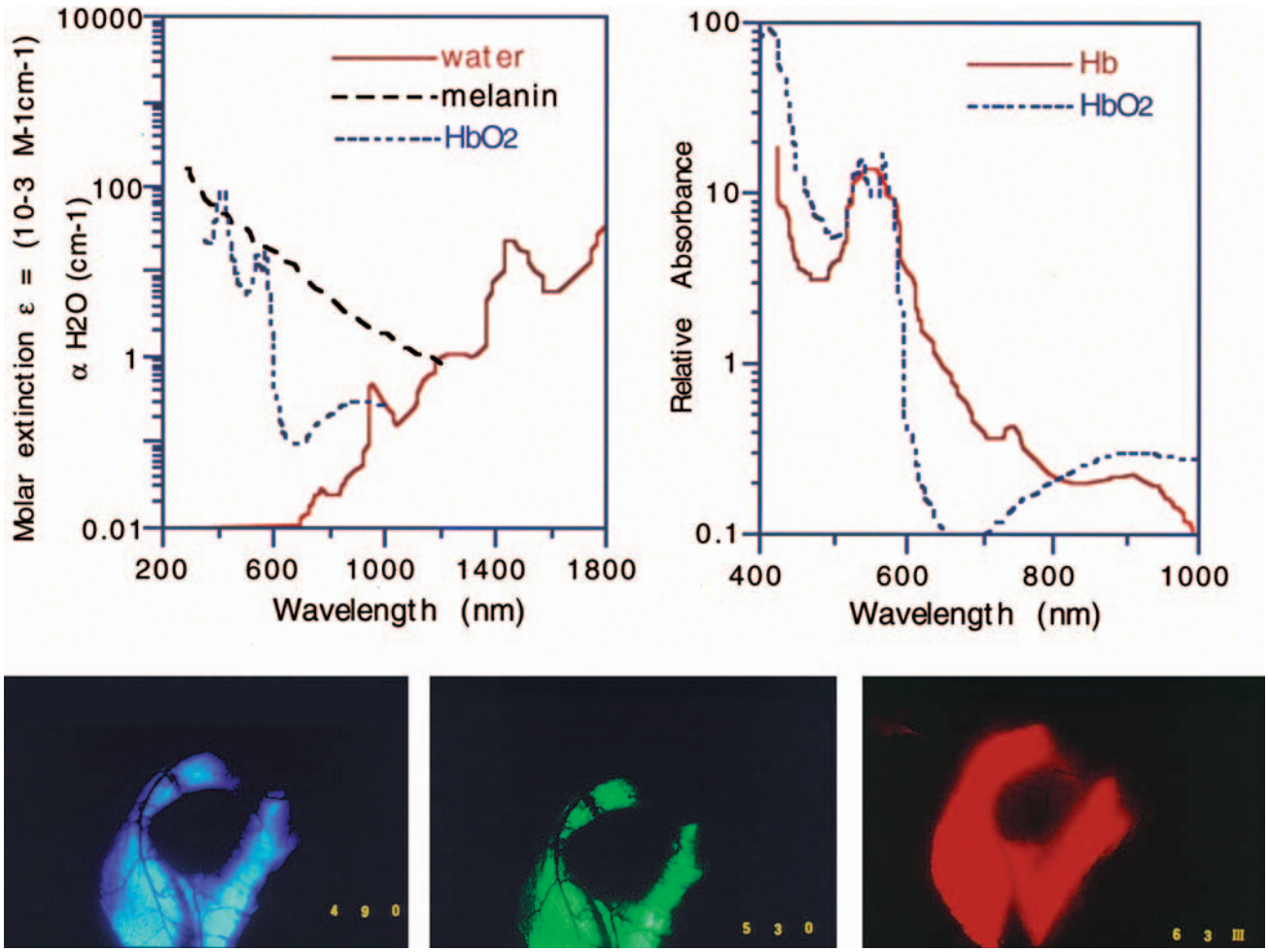


**Figure 1.** *Upper panels: Spectral dependence of tissue chromophore absorption. A tissue optical "window" exists in the red/NIR between 600 and 1300 nm (from J.L. Boulnois, Lasers in Medical Science, 1986: 1: 47–66). Lower panels: Spectral dependence of light transmission through rabbit ear with implanted tumor model.*

Figure 1 illustrates that within the visible (300 to 700 nm) water window, hemoglobin and melanin are the dominant endogenous absorbers [4].

Although melanin absorption coefficients are, on average, greater than those of hemoglobin, the overall influence of melanin on light propagation in thick tissues is generally less substantial. This is due to the fact that melanin is typically confined to a thin, superficial skin layer. In contrast, hemoglobin is widely distributed throughout most tissues at a volume fraction that ranges from 1% to 5%. Exceptions to this include avascular structures and tissues with abnormally high melanin content, such as melanotic melanomas.

Scattering originates from inhomogeneities in tissue structure, which, in turn, are determined by refractive index discontinuities occurring both between and within cells. In the spectral region of 600 to 700 nm, hemoglobin absorptivity is attenuated by approximately 20 dB (nearly 100-fold) and scattering eclipses absorption. This condition persists until water absorption resumes as the primary attenuation mechanism at approximately 1.3 $\mu$m. Thus, the spectral region between 600 and 1300 nm is considered to be the tissue optical "window" since both absorption and scattering losses are minimal throughout this interval. This concept is illustrated in the series of three photographs shown at the bottom of Figure 1. Here, a rabbit ear implanted with a tumor model is transilluminated using blue (490 nm), green (530 nm) and red (630 nm) light. In the blue and green photographs, excellent contrast is observed between light-absorbing blood vessels and the surrounding ear cartilage. This is due to strong hemoglobin absorption in these spectral regions and relatively high attenuation of light from scattering. Because the tumor has substantial blood vessel/hemoglobin content, it appears as a large light-absorbing shadow. In the red light case, however, the image appears quite diffuse and the small vessel structures have disappeared. This is a consequence of the substantially reduced hemoglobin absorption at 630 nm, making these vessels appear to be "transparent". In addition, red light is scattered less than blue/green. As a result, many of the scattered photons contribute to the image as "multiply scattered light," further degrading spatial resolution and contrast while improving transparency. The net result is a "cloudy" tumor that appears to be different than its actual physical dimension.

The wavelength-dependent intensity of light penetrance into biological tissues can be used to characterize structures of different composition. Table 1 provides several practical examples of wavelength-dependent "optical penetration depths", $\delta$, a value that corresponds to the distance at which the optical fluence rate (i.e., mW/cm$^2$) is reduced to $1/e$=0.37 of the initial value [5]. These data highlight the dynamic interplay between absorption and scattering. For example, since human retinoblastomas contain no melanin, low levels of hemoglobin, and are only minimally scattering, penetration depths are relatively large; ranging from 2.9 mm at 600 nm to 5.1 mm at 1.06 $\mu$m. Light penetrance is commensurately reduced in brain and hand tissue due to their high-scattering/low-absorption and moderate-scattering/moderate-absorption properties, respectively. In contrast, the high melanin content of melanotic melanomas strongly attenuates light throughout the visible region and maximum light penetrance is only 1.4 mm at 1.064 $\mu$m.

These examples indicate that, in general, $\delta$ for non-melanotic tissues follows hemoglobin absorption. Thus, from 480 to 590 nm, $\delta$ ranges from 0.5 to 1.5 mm. A substantial penetration depth increase from about 1 to 3 mm occurs between 600 and 650 nm, and a more gradual increase is observed from 650 to 750 nm ($\delta$=2 to 4 mm). Between 750 and 900 nm, values tend to plateau, and maximum light penetrance of 3 to 6 mm generally occurs in the 1000 to 1100 nm region.

*Multiple Scattering*

On a cellular level, there are clear, visible differences between normal and malignant tissues. These changes may include, among others, multinucleation, structural distortion, hyperpigmentation, and membrane and mitochondrial variations. On a bulk tissue level, there are distinct variations in tumor vasculature, extracellular matrix and biochemical milieu. Pathologists utilize visible, microscopic anomalies in cell/tissue architecture to formulate diagnoses. Thus, variations in bulk tissue optical penetration depths are expected, given the large body of supporting histologic evidence [6]. These fundamental optical property differences can, in principle, provide novel diagnostic criteria for thick-tissue photon migration methods.

However, our ability to employ thick-tissue optical methods for cancer detection is limited by a form of light-scattering behavior known as "multiple scattering". Light launched into tissue is efficiently scattered out of an incident collimated beam into an almost isotropic distribution within a few millimeters from the source. This "multiple scattering" behavior degrades the information content of light that propagates through thick tissues. In practical terms, optical imaging methods that cannot distinguish between scattering

**Table 1.** Optical Penetration Depth (mm) as a Function of Wavelength (From Ref. [5]).

| Tissue | Wavelength (nm) | | | | | | | |
|---|---|---|---|---|---|---|---|---|
| | 600 | 650 | 700 | 750 | 800 | 850 | 900 | 1064 |
| Human retinoblastoma (*in vitro*) | 2.9 | 3.8 | 4.0 | 4.0 | 4.1 | 4.2 | 4.3 | 5.1 |
| Porcine brain (*in vitro*) | 1.8 | 2.4 | 2.9 | 3.0 | 3.3 | 3.5 | 3.7 | 4.0 |
| Human hand (*in vivo*) | 1.4 | 2.0 | 2.6 | 2.7 | 3.0 | 3.0 | 3.0 | – |
| Melanotic melanoma in athymic mice | – | 0.28 | 0.34 | 0.41 | 0.50 | 0.56 | 0.64 | 1.4 |

and absorption are incapable of providing a complete diagnostic picture. This concept is illustrated schematically in Figure 2.

In homogeneous, non-scattering media, light propagation is simply a function of the absorption coefficient, $\mu_a$, and distance, $z$:

$$I = I_0 e^{-\mu_a z} \quad (1)$$

where $\mu_a = 1/l_{ab}$ and $l_{ab}$ is the absorption length, or average distance between absorption events. The absorption coefficient can be expressed in terms of molecular concentration via the Lambert-Beer law (i.e., $A = \log I/I_0 = \varepsilon bC$, where $A$, $\varepsilon$, $b$, are $C$ are absorbance units, molar extinction coefficient, pathlength, and molar concentration, respectively):

$$\mu_a = 2.3\varepsilon C \quad (2)$$

Thus, measurements of light penetrance in tissues can, in principle, provide quantitative information regarding the concentration of physiologically relevant absorbers.

However, in non-transparent, turbid media, both scattering and absorption contribute to the distance-dependent light attenuation. The total attenuation coefficient, $\mu_t$, is the sum of absorption and scattering parameters ($\mu_t = \mu_a + \mu_s$). Here, $\mu_s$ is the scattering parameter, or the reciprocal of the scattering length ($l_{sc}$). In the special case of "multiple scattering", the incident light intensity diminishes according to:

$$I = I_0 e^{-\mu_{eff} z} \quad (3)$$

where the effective attenuation coefficient, $\mu_{eff} = 1/\delta = [3\mu_a(\mu_a + \mu_s')]^{1/2}$ is the reciprocal of the mean penetration depth ($\delta$). In order to account for multiple scattering, the reduced scattering parameter, $\mu_s' = \mu_s(1-g)$ is defined in terms of $\mu_s$ and the angular dependence of scattering, $g$, where $g = \langle \cos theta \rangle$, (i.e., the average cosine of the scattering angle). In most tissues, scattering is highly forward-directed and $g$ values range from 0.7 to 0.9 [6]. In practical terms, large $g$ values delay the distance photons must travel before optical energy is isotropically distributed. Generally, this "transport mean free path" (tmfp) is on the order of 1 mm in most tissues and can be defined as the reciprocal of the transport scattering coefficient, $\mu_{tr} = \mu_a + \mu_s'$.

*The Diffusion Approximation*

In order to probe large volumes of tissues with acceptable signal-to-noise levels, measurements are generally conducted in spectral regions of greatest transparency, i.e., the tissue optical window (600 to 1300 nml see Figure 1). Under these conditions, scattering dominates absorption and light propagation can be described by a diffusion approximation [12,21]. Since scatterers and absorbers are distributed in

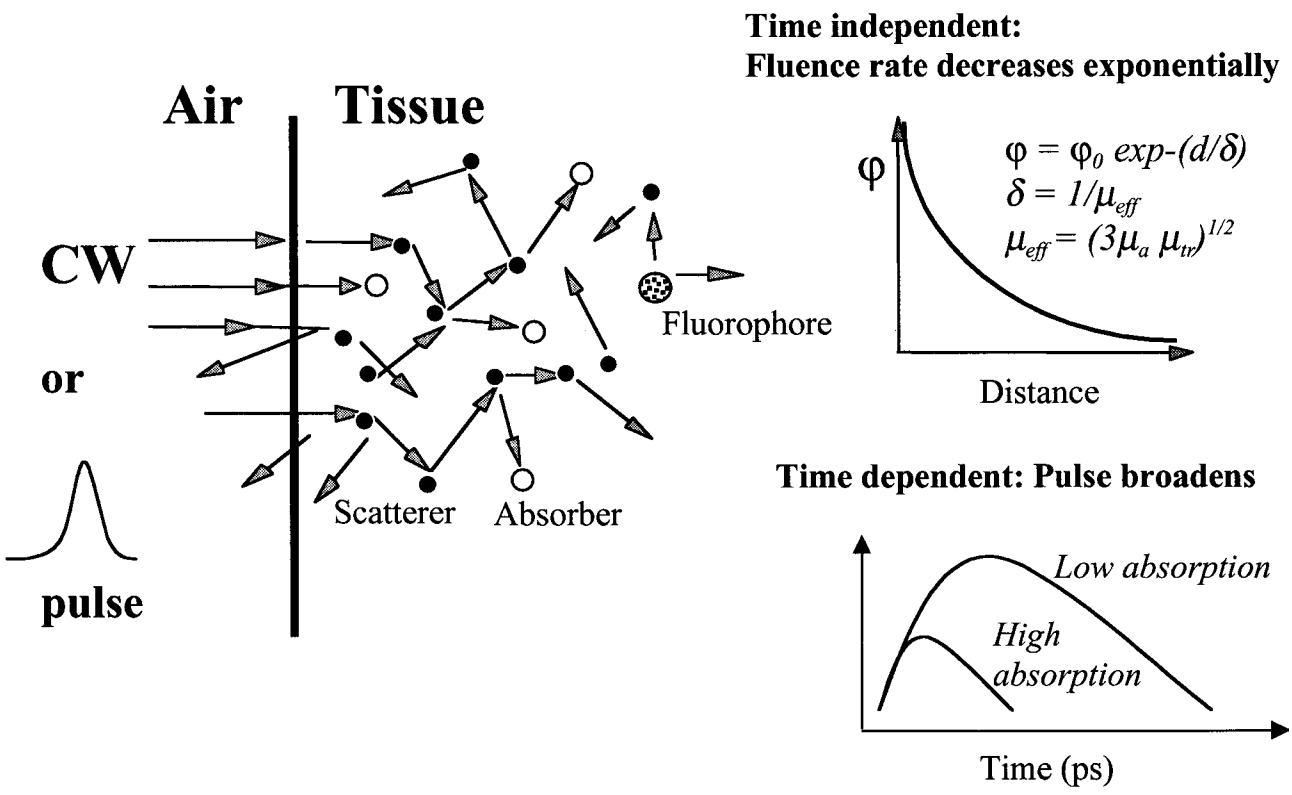


**Figure 2.** *Red/NIR light launched into tissue propagates with directional changes (scattering) until captured by an absorber (molecule). Multiple scattering increases the mean photon path length. A short, e.g., picosecond, light pulse launched into tissue spreads out in proportion to the number of available photon paths. Absorption is a loss mechanism that reduces the number of available photon paths and hence limits the temporal dispersion of the pulse. Under low absorption conditions, a light pulse will experience maximal dispersion. The photon density, or fluence rate ($\varphi$) decays exponentially with distance from the source. The 1/e exponential decay constant, or optical penetration depth ($\delta$) is a function of the absorption, $\mu_a$, and scattering, $\mu_s'$, properties of the medium.*

tissues on dramatically different spatial scales (i.e., $\mu_s'z.Gt\mu_a$), the transport scattering length can be approximated by $1/\mu_{tr} \approx 1/\mu_s'$. Under these conditions, an additional descriptive domain, i.e., time or frequency, is required to resolve light scattering from absorption.

As shown in Figure 2, launching light into tissue results in multiple scattering events that can dramatically increase the mean path length beyond the linear distance from source to detector. If the light source continuously illuminates the sample (i.e., it is time-independent), the fluence rate (in $mW/cm^2$) or number density of photons measured in the sample from all directions decays exponentially with distance from the source. The decay rate is a function of the penetration depth, $\delta$, which in turn can be given by the absorption and scattering properties. When a time-dependent light source is used such as a picosecond (psec) laser pulse or a sinusoidally intensity-modulated laser, the large number of photon paths available due to multiple light scattering processes causes broadening of the source temporal profile. Thus, measurements of the time-dependent propagation characteristics of short light pulses or intensity-modulated waves in tissues can be used to separate the contributions of absorption from scattering. When combined with an appropriate mathematical framework, this allows precise calculation of tissue optical properties, namely tissue absorption, $\mu_a$, and reduced scattering, $\mu_s'$, properties.

*Temporal Resolution*

Over the past few years, remarkable gains in our understanding of tissue optical properties have been realized by interrogating tissues with the unique temporal (i.e., short pulse) properties of lasers [7–11]. Pulse propagation methods provide information about the distribution of scatterers and absorbers in a single measurement [12,13]. These optical properties may be used in a variety of therapeutic and diagnostic techniques, including: imaging tissue structure [14–16] and cortical activity [17,18]; monitoring physiology [19–23] and drug concentration [24]; dysplastic transformation [25], and predicting optical dosimetry for laser-based procedures [26].

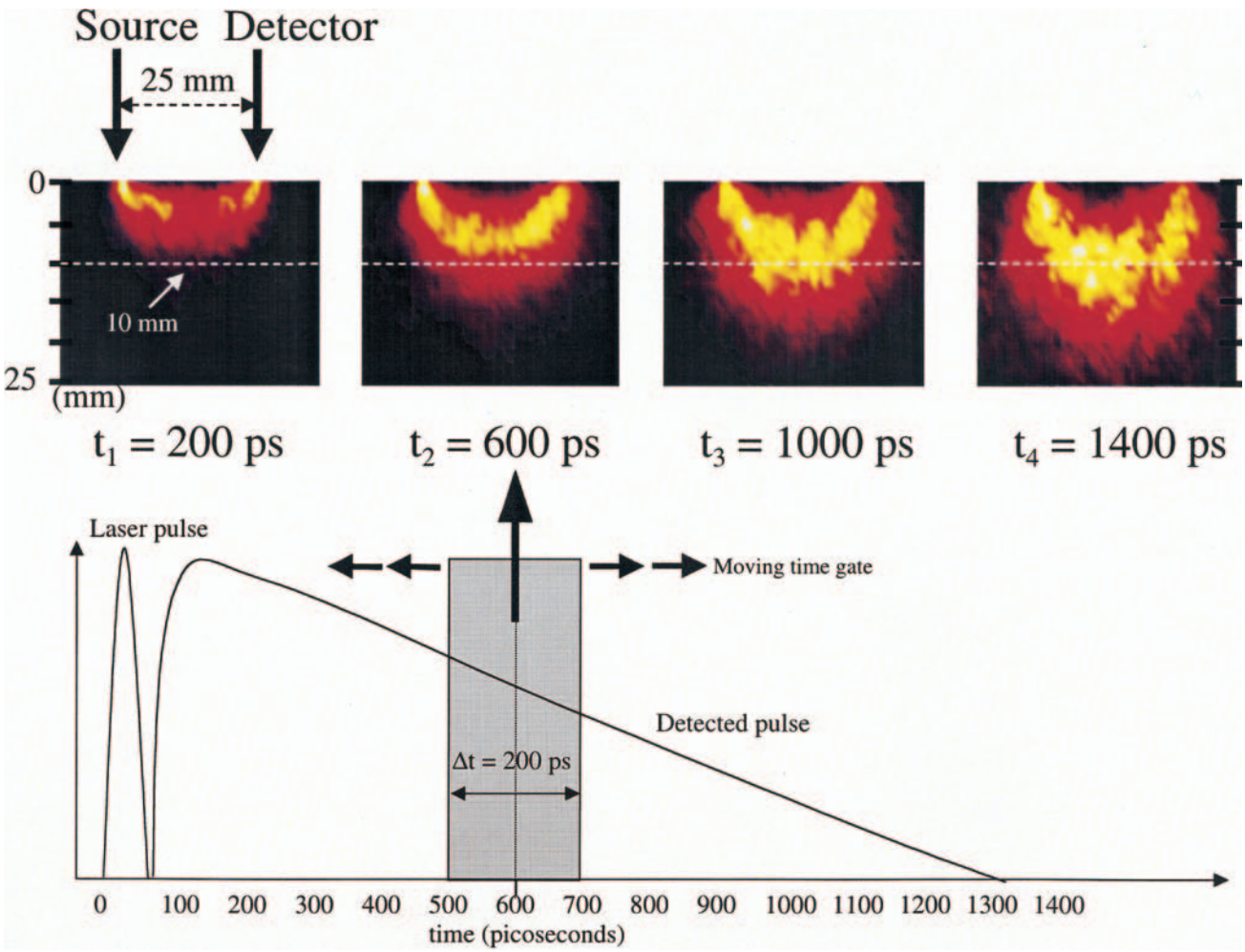


**Figure 3.** *Numerical simulation showing time-dependent propagation of ultrashort light pulse in tissue with optical properties similar to human breast ($\mu_a = 0.1\ cm^{-1}$, $\mu_s' = 10\ cm^{-1}$). Two-dimensional x–z views ($40 \times 25\ mm^2$) of detected photon density are shown. Time-gating of the detector provides control over depth and volume of tissue probed.*

The conceptual basis for the time-domain approach generally involves solutions to the radiative transfer equation [27,28] using Monte Carlo simulation [29–31] and diffusion theory approximations [7,32]. Diffusion-based methods provide relatively straightforward analytical expressions that describe the shape of a diffusely reflected or transmitted pulse in terms of the optical properties of the medium [10]. Thus, the observed temporal broadening of ultra short pulses can be mathematically related to the large number of optical paths available in multiple-scattering media. Since the introduction of losses (absorbers) reduces the average path length, absorber-dependent changes in pulse propagation time can be used to calculate absorption coefficients [10]. This concept is illustrated in Figure 3. Here, a picosecond light pulse is launched into a tissue-like medium with optical coefficients similar to human breast tissue ($\mu_a$=0.1 $cm^{-1}$, $\mu_s'$=10 $cm^{-1}$). The transport characteristics of the source are simulated numerically using a Monte Carlo technique [33]. The figure shows how the detected pulse spreads out in time and space, due to the large number of photon paths available. By time-gating the detector, one can adjust the "viewing volume" in the tissue. For example, at early times after the pulse is launched, shorter photon paths are detected. This is demonstrated by the 200 psec time point that samples tissue volumes above the 1 cm depth line. When the 200 psec observation "gate" is shifted to $t$=600 psec, the mean interrogation depth and volume are substantially greater. This is due to the fact that at longer times, photons have traveled tens of centimeters, substantially further than the 2.5 cm linear distance between source and detector. By moving the observation window through the time course of the detected signal, the spatial distribution of absorbers and scatterers in the tissue can be reconstructed, and sensitivity to deep tissue structures, such as tumors, can be optimized.

Frequency-domain optical methods can be adapted to diffusion theory models in a similar manner. Fishkin and Gratton [34] first suggested that amplitude-modulated light propagates through homogeneous multiple-scattering media as diffuse waves with a coherent front. These photon density waves can be characterized by a phase velocity ($V_p$) and modulation wavelength ($\lambda_m$) that are primarily functions of media optical properties. Measurements are performed by launching intensity-modulated light into tissue and recording the phase delay (*phi*) and demodulation amplitude ($m$) (with respect to the source) at a fixed distance from the launch site. Optical properties (the absorption coefficient, $\mu_a$, and the reduced scattering coefficient, $\mu_s'$) are calculated from the measured frequency- and distance-dependent behavior by fitting the experimental results to an appropriate theoretical framework. Thus, FDPM can rapidly and quantitatively assess tissue optical properties in a single non-invasive measurement. It is important to point out that time and frequency domain methods are equivalent and related to each other through the Fourier transform. We employ the frequency-domain approach due to instrumentation advantages that include reduced cost, complexity, and simplicity of mathematical techniques used in frequency-domain signal analysis [35].

**Instrumentation**

In frequency-domain photon migration (FDPM), the intensity of light incident on an optically turbid sample is modulated at high frequencies (e.g., hundreds of megahertz), and the diffusely reflected, transmitted, or re-emitted (e.g., fluorescent) signal is measured with a phase-sensitive detector. Intensity-modulated light propagates through multiple-scattering media with a coherent front, forming photon density waves (PDWs). PDW dispersion is highly dependent on the optical properties of the medium. Exact absorption ($\mu_a$) and reduced scattering ($\mu_s'$) parameters are calculated by comparing the measured frequency- or distance-dependent PDW phase and amplitude behavior to analytically derived non-linear model functions. Model functions are, in turn, derived from solutions to the photon diffusion equation which yield expressions for phase (*phi*) and amplitude ($A$) as a function of modulation frequency ($\omega$) and tissue optical properties under various boundary conditions [36]. The values *phi*, $A$, and $\omega$ are defined in the usual manner where *phi*=the measured phase lag between the source (reference) and sample response; $A=AC_{sample}/AC_{source}$; and $\omega=2\pi f$ is the angular modulation frequency.

A schematic of our 1-GHz, portable FDPM device is shown in Figure 4 [37]. FDPM instrumentation and theoretical background have been described in detail elsewhere (Fishkin et al. [41]; Chance et al. [35]). Briefly, modulation is swept from 300 kHz to 1 GHz in less than 1 second, providing rapid, multi-wavelength (~670 to 960 nm) characterization of most tissues in a single measurement. The instrument is compact and can easily be transported to operating rooms and bedridden patients. By incorporating several NIR laser diodes, a number of wavelength-dependent physiological parameters are determined. Source modulation frequencies typically range from 300 kHz to 1 GHz, with FDPM data recorded in 5 MHz increments.

The core component of the FDPM apparatus is a network analyzer (Hewlett Packard, model 8753C), which is used to produce modulation swept from 300 kHz to 1 GHz (20 dB m RF output). RF from the network analyzer is serially superimposed (via the AC switch) on the direct current of up to eight different diode lasers (e.g., SDL, Inc. models 7421, 5420, 5421, and 6321 at 674, 811, 849, and 956 nm, respectively) using individual bias-tees (model 5575A, Picosecond Pulse Labs) and an RF switch (model 8768K, Hewlett Packard). One-hundred-micrometer-diameter gradient-index fibers are used to couple each light source to an 8×8 optical multiplexer (model GP700, DiCon Instruments). The 8×8 optical multiplexer allows for up to eight different diode laser light sources and eight different optical fiber positions.

Light is launched onto the tissue (or test object) using the above-mentioned unique wavelengths and one source fiber.

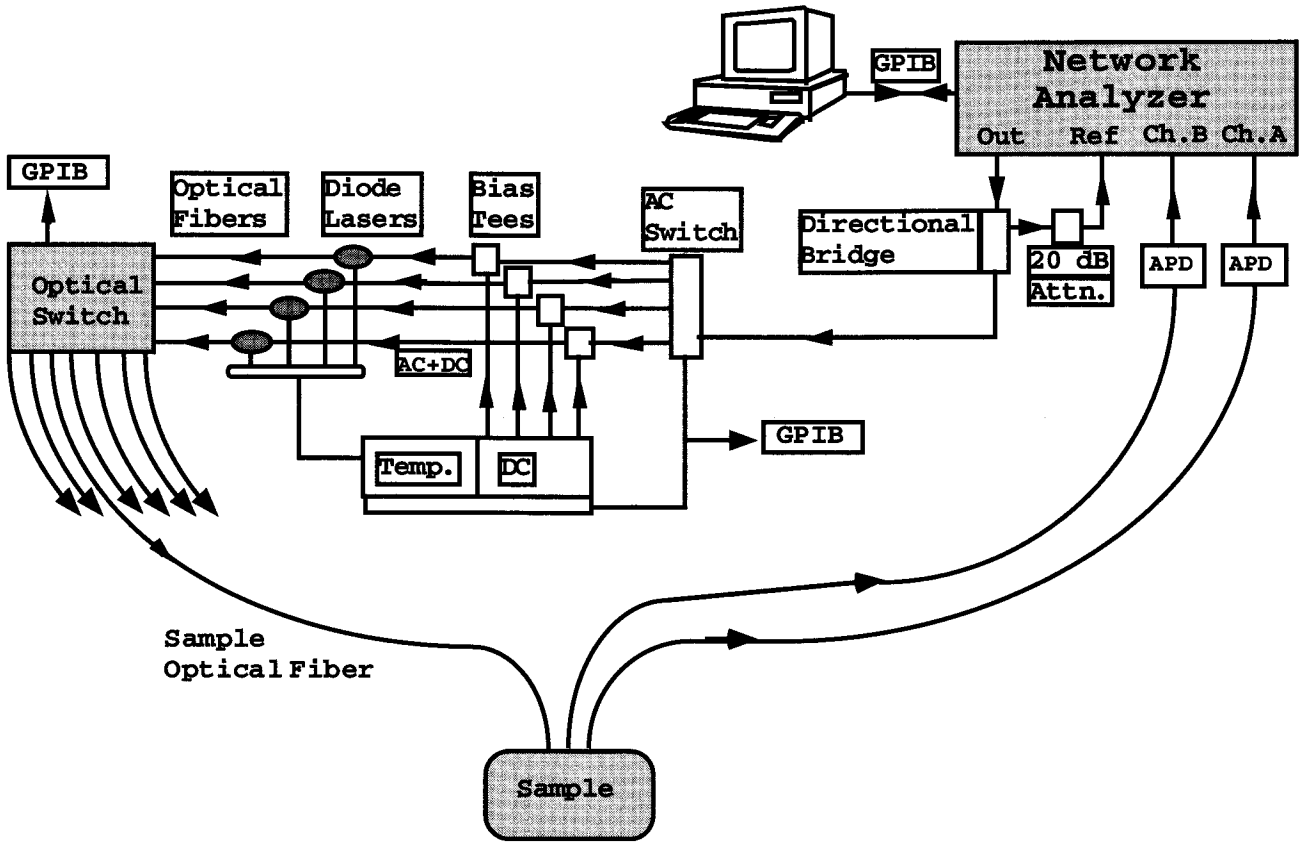


**Figure 4.** *One-gigahertz, multi-frequency, multi-wavelength FDPM instrument. See text for complete description.*

An avalanche photodiode (APD, Hamamatsu, model C5658) is used to detect the diffuse optical signal that propagates through the biological tissue. Both the APD and probe end of the source optical fiber are in direct contact with the patient (i.e., a "semi-infinite medium" measurement geometry). The optical power coupled into the tissue averages approximately 10 to 30 mW. Measurement time depends on the precision required, the number of sweeps performed, and RF/optical switch times. For human subject studies, approximately 0.1 second is used to sweep over the entire 1 GHz band of modulation frequencies. However, total elapsed time for four diodes (typically 12 to 16 sweeps/diode), data transfer, display, and source switching is approximately 40 seconds. Most components, including the network analyzer, RF/optical switches, diode power supplies and temperature of diode mounts are controlled by computer using virtual instrument software (LabView, National Instruments).

As shown schematically in Figure 5, phase and amplitude data (represented by *phi* and *A*, respectively) obtained from frequency-dependent FDPM tissue measurements are fit to theoretical model functions. This results in calculation of the optical absorption coefficient, $\mu_a$, and the reduced scattering coefficient, $\mu_s'$, at a given $\lambda$ and source–detector separation $\rho$. Minimization of the $\chi^2$ surface is achieved for simultaneous, error-weighted fitting of the *phi* and *A* versus frequency data using a Marquardt-Levenberg algorithm. Typical $\mu_a$, and $\mu_s'$ uncertainties, determined from the $\chi^2$ distribution of phase and amplitude fits, range from 0.5% to 5% of the mean value. When optical properties ($\mu_s'$ and $\mu_a$) are recovered for various source wavelengths, the spectral dependence of absorption can be combined with known values of molecular extinction coefficients to calculate physiologically relevant parameters, such as oxygenated, deoxygenated, and total hemoglobin concentration; oxygen saturation; drug concentration; blood volume fraction; and water concentration. The spectral dependence of scattering is used to provide insight into the mean density and size of scattering structures.

**Application to Solid Tumor Characterization**

The sensitivity of optical properties to tissue structure and function suggests that differences between normal and diseased tissues may provide a means for assessing the probability that processes such as malignant transformation, inflammation, or infection are occurring. Indeed, previous studies have shown unique scattering and/or absorption signatures associated with dysplastic [25,38,39], malignant [41] and benign [45] tissue transformations.

Characterization of solid tumors in thick tissues poses unique challenges. These structures are typically found embedded beneath epithelial layers and require methods capable of probing deep tissue structure and function.

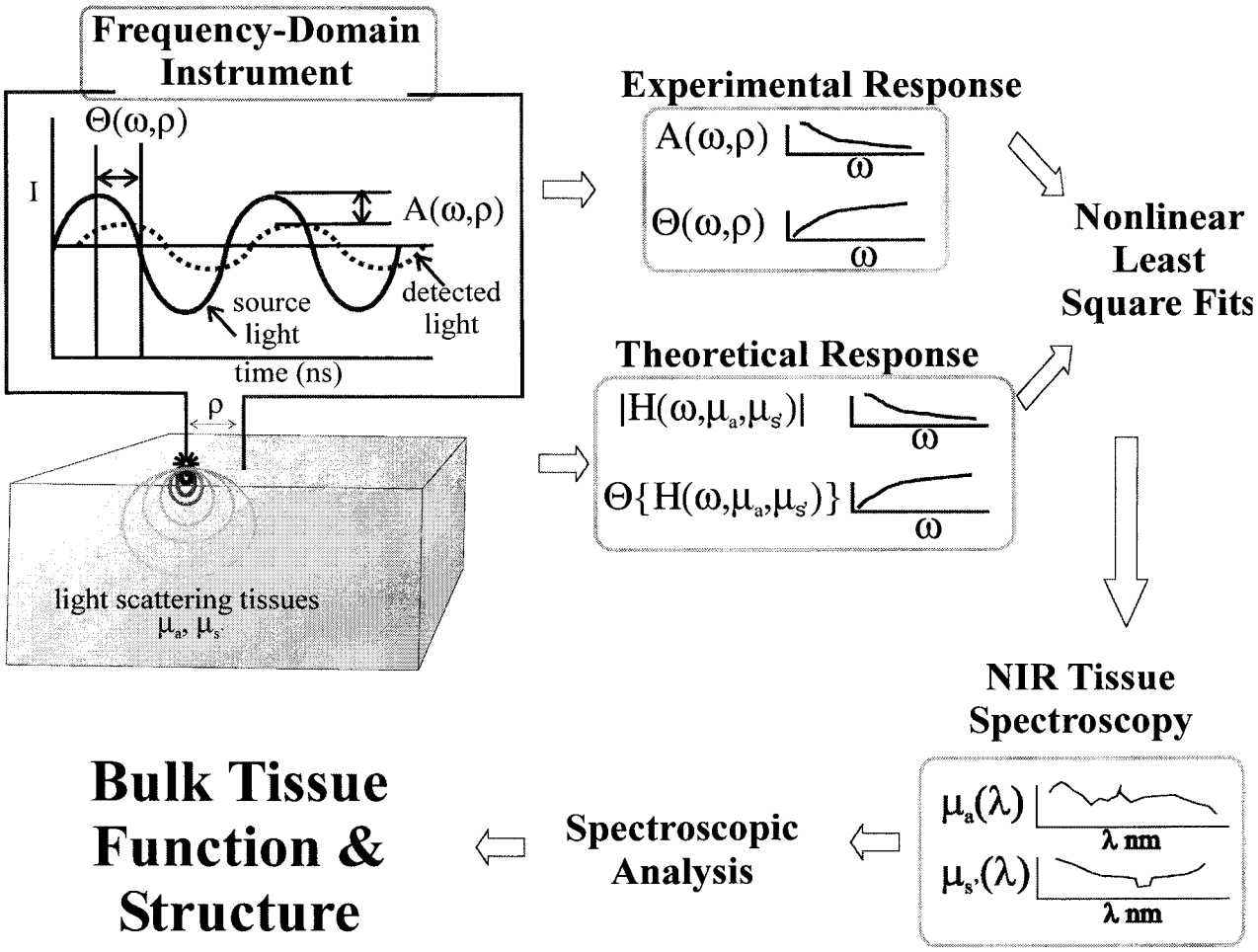


**Figure 5.** *FDPM measurement overview: intensity-modulated light is launched into tissue, resulting in the propagation of diffuse photon density waves. The frequency-dependent experimental response (phase, phi, and amplitude, A vs. frequency, $\omega$) is compared to a theoretical model. Model-data fits provide calculated values for absorption, $\mu_a$, and reduced scattering, $\mu_s'$, coefficients at each optical wavelength. Absorption and scattering spectra are generated. Absorption spectra are used to calculate concentration of principal tissue chromophores.*

Because of multiple light scattering, spatial resolution using "diffuse methods" is intrinsically rather poor, on the order of 1 to 5 mm [40]. Nevertheless, imposing temporal resolution can confine the photon interrogation volume to specific regions (see Figure 3) and improve sensitivity to buried tumors. This is achieved by examining the temporal point spread function of a short light pulse, as illustrated in Figure 3, or by measuring the phase and amplitude of photon density waves, as illustrated in Figure 5. By measuring *phi* and *A* at multiple modulation frequencies ($\omega$), information that is comparable to recording the temporal profile of the diffusely propagating pulse is obtained. When these data are recorded at multiple wavelengths ($\lambda$), FDPM becomes a quantitative spectroscopic technique.

Structural components that contribute to FDPM signals in thick tissues are shown in Figure 6*A*. The appearance and progression of tumors alter the fractional contribution of cells, extracellular matrix, and vasculature to the absorption and scattering spectra. In addition, spatial variations in optical properties may be evident for poorly differentiated tumor versus well-differentiated normal tissues. This is due to the fact that, with disease progression, there is typically an increase in tumor cell density, nuclear volume fraction, and stromal/inflammatory cells. Extracellular matrix degrades with increasing tumor invasion, and neovasculature is recruited, forming a tortuous, leaky network complete with flow anomolies. These alterations in tissue architecture affect both the absolute value and wavelength dependence of the reduced scattering parameter. From a molecular perspective, we assume that the chromophores contributing to $\mu_a$ at a given NIR wavelength are principally oxy- and deoxy-hemoglobin, water, and fat. The total absorption measured at a given wavelength is a linear sum of each. Thus, in order to achieve optimal sensitivity, it is desirable to illuminate the tissue with light source wavelengths that correspond to high-contrast absorption features. For example, in Figure 6*B*, fractional spectral contributions are shown for physiological concentrations of principal components in a typical breast tissue: deoxy- and oxy-hemoglobin, fat, and water. Sources at about 670, 810, 920, and 960 nm are most

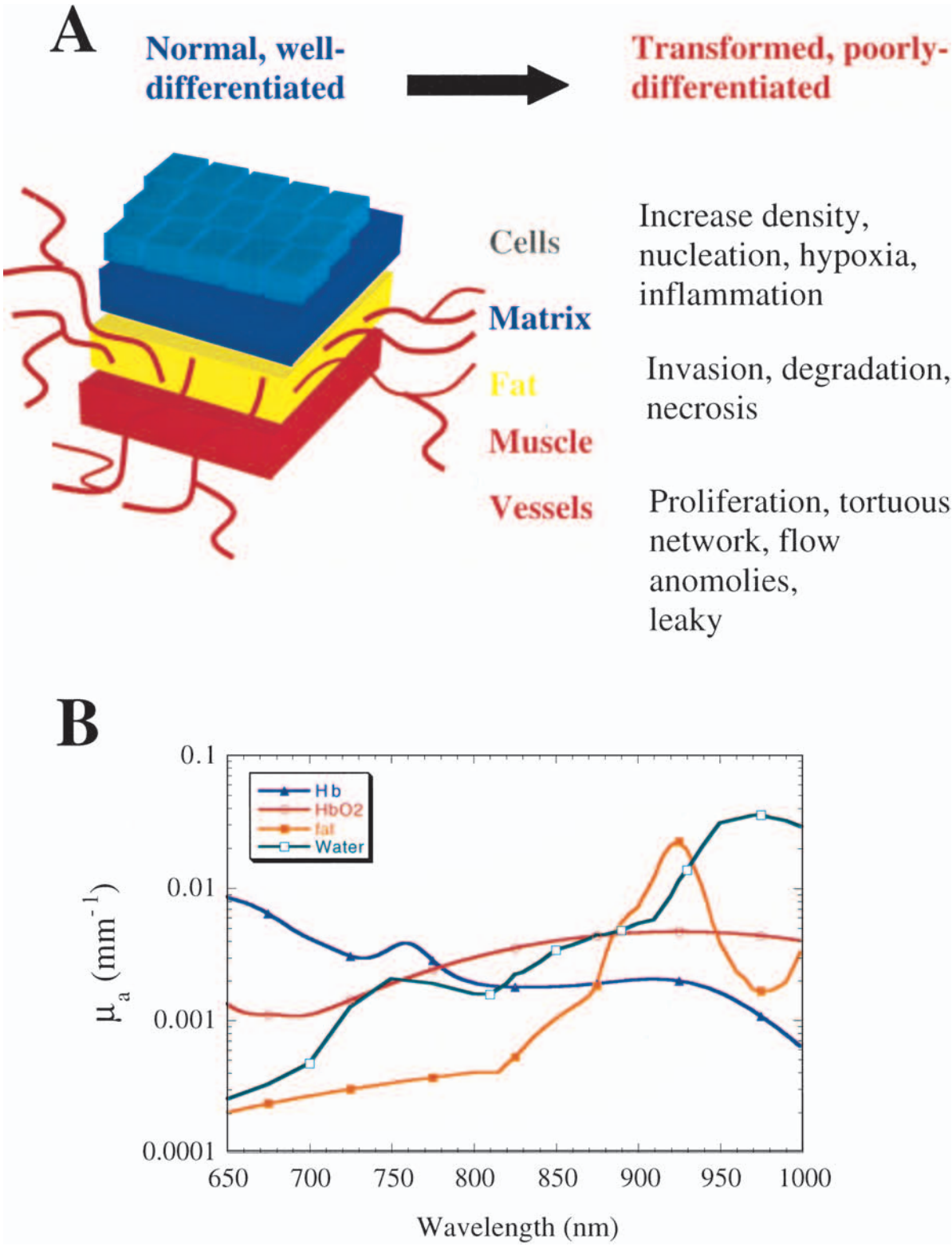


**Figure 6.** *(A) Structural and functional components of the optical signal in normal and transformed tissue. (B) Absorption spectra of tissue with composition similar to human post-menopausal breast: 10 μM deoxyhemoglobin [Hb], 15 μM oxyhemoglobin [$HbO_2$], fat (80% volume fraction), and water (15% volume fraction).*

sensitive to each. In order to calculate tissue concentrations, $\mu_a$ measurements at a minimum of four different wavelengths are combined with known values of molecular extinction coefficients [41]. Due to the metabolic demands of rapidly proliferating tumor cells and increased tumor vasculature, these biochemical constituents can vary substantially in relative abundance for normal versus diseased tissue.

*Breast Measurements: Results and Discussion*

The relative impact of these physiological features on photon migration can be determined by examining normal breast tissue optical properties (see Ref. [42] for a description of breast tissue optics). Figure 7 shows results of FDPM measurements obtained from two pre-menopausal and two post-menopausal subjects (27, 29 and 63, 67 years old, respectively). Data were collected from the right upper outer quadrants of each subject while in a reclining position. The probe was applied with gentle pressure (i.e., no external compression) using a source–detector separation of 2.5 cm.

Pre- and post-menopausal normal breasts exhibit clear wavelength-dependent differences in both absorption and scattering parameters. Figure 7*B* shows that scattering is approximately 20% greater in pre-menopausal ($\mu_s'$~0.8 to 1.1 $mm^{-1}$) versus post-menopausal women ($\mu_s'$~0.6 to 0.7 $mm^{-1}$). In addition, the wavelength dependence of scattering is steeper for pre- versus post-menopausal subjects. These findings are consistent with known changes in breast physiology. Breast tissue, while under hormonal control, has higher glandular/cellular content and collagen is required in the extracellular matrix in order to support the structural demands of cellular proliferation. After menopause, the absence of hormonal stimulation results in glandular shrinkage, collagen remodeling to fat, and diminished vasculature. Since small tissue structures such as collagen fibers and subcellular organelles are likely to be the primary contributors to tissue scattering, it is not surprising that the wavelength dependence of scattering is relatively steep for pre-menopausal subjects. In contrast, following conversion to a principally large-particle fatty matrix, a much more gradual wavelength dependence of scattering is observed. Thus, the diminished contribution of the glands and collagenous stroma leads to a clear wavelength-dependent scattering reduction.

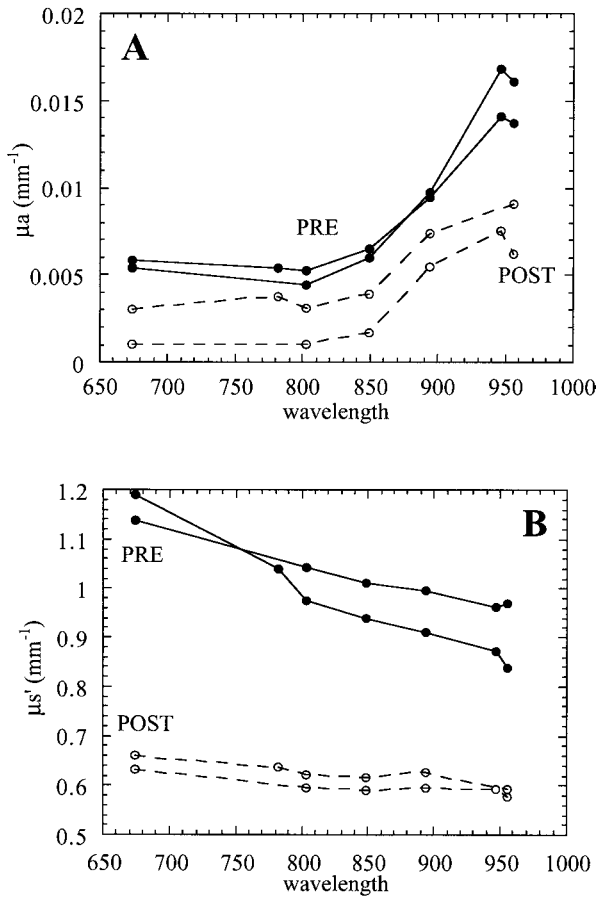


**Figure 7.** *FDPM measurements in PRE (●) and POST (○) menopausal normal breast (four subjects). (A) Calculated values of absorption coefficients, $\mu_a$, vs. wavelength. (B) Calculated values of reduced scattering coefficients, $\mu_s'$, vs. wavelength.*

Variations in absorption can be explained in a similar manner. Absorption contrast due to enhanced perfusion is clearly detectable while breast tissue is under hormonal control. This is reflected in Figure 7*A* values of absorption coefficients that are consistently higher for pre-menopausal subjects. Following menopause, the absence of substantial metabolic demand leads to reduced perfusion and lower absorption values. This is well-correlated with the low blood, high fat content of post-menopausal tissue. Similar changes in optical properties have been observed by others [43,44].

These results demonstrate the intrinsic sensitivity of FDPM to breast tissue physiological states. In order to address the origin of photon migration signals in solid tumors, we have initiated breast tumor studies in human subjects [45]. Our goal is to carefully define the level of accuracy and precision required from our measurement techniques so that malignant lesions can be identified and resolved from normal structures with a reasonable level of confidence. The practical impact of increasing diagnostic specificity would be two-fold: 1) enhanced early detection of relatively small (0.5 to 1 cm diameter) tumors is likely to lead to mortality improvements (mammographic performance is highly variable in pre-menopausal subjects); and 2) more specific characterization of benign versus malignant lesions would lead to reductions in the large number of unnecessary surgical biopsies. As a result, there is considerable room for the development of new, non-invasive optical methods for characterizing breast tissue.

In the following discussion, we present results from three individuals. Experiments were performed under the guidelines of UC Irvine IRB-approved protocol #95-563. Patient 1 was a 67-year-old post-menopausal subject with a single palpable mass 7.4 mm beneath the skin surface in the upper outer quadrant of the left breast. Histological examination following surgical biopsy and ultrasound revealed a 1.8×0.9 cm ductal carcinoma in situ (DCIS) (malignant tumor). Patient 2 was a 63-year-old post-menopausal subject with a non-palpable spiculated left breast mass. Histological examination following surgical biopsy revealed a 0.6×0.4×0.7 cm invasive ductal carcinoma (malignant tumor). Patient 3 was a 22-year-old, pre-menopausal subject patient with a 2×2 cm palpable mass 3–7 mm below the surface in the upper medial portion of the right breast. Surgical biopsy revealed the presence of a benign fibroadenoma.

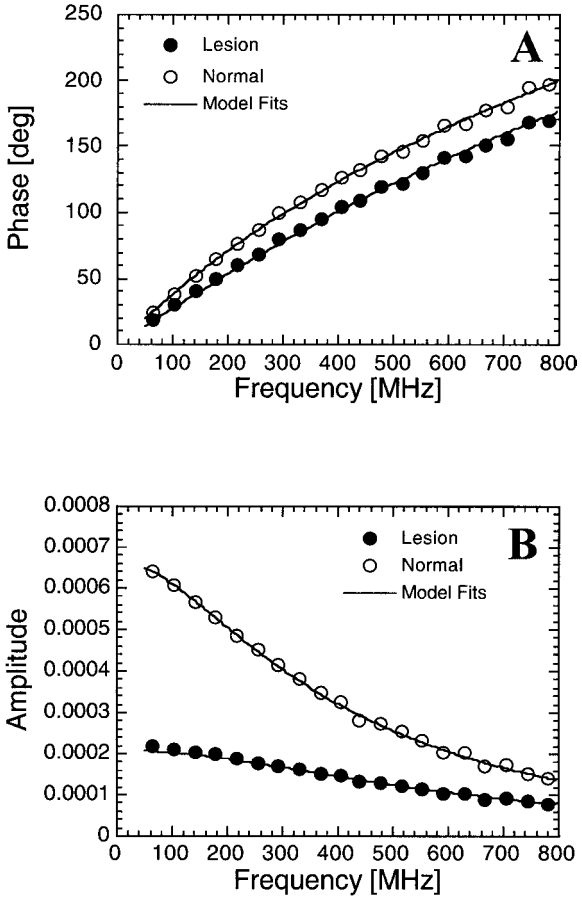


**Figure 8.** *FDPM measurements of phase (A) and amplitude (B) vs. source modulation frequency obtained from normal and tumor sites on patient 1 (ductal carcinoma in situ, DCIS). Source–detector distance = 2.5 cm; $\lambda$ = 674 nm. Solid lines are best simultaneous fits to phase and amplitude data from tumor (●) and normal (○) data points, respectively. Ten percent of 200 frequency-domain data points is shown for clarity.*

Measurements are performed on each patient by gently placing the FDPM probe on both normal and tumor-containing breast. Data are acquired using a hand-held scanning probe placed in nine discrete locations covering a 2×2 $cm^2$ grid mapping the breast surface. The probe incorporates source–detector (s–d) pairs ranging from 1 to 2.5 cm in separation. The 2.5 cm s–d configuration is placed on the tissue with the source and detector bracketing the tumor. Tumor location, dimension, and depth are monitored immediately prior to FDPM measurements by ultrasound. Photon migration data are acquired by moving the probe in 0.5 mm increments along inferior–superior and medial–lateral paths. Repeat measurements immediately above tumor center are obtained at least three times. Both normal and tumor-containing breasts are studied. Each tissue location is characterized in terms of wavelength-dependent absorption and scattering parameters which, in turn, are used to calculate physiological properties.

Sequential scans of the same location following probe removal and replacement revealed no significant variations in optical properties. Normal tissue measurements are acquired in the same manner from a symmetric site on the opposite, uninvolved breast. Phase and amplitude data (represented by *phi* and *A*, respectively) obtained from FDPM tissue measurements are compared to semi-infinite model functions to extract the optical absorption coefficient, $\mu_a$, and the reduced scattering coefficient, $\mu_s'$, at a given $\lambda$ and source–detector separation. Typical $\mu_a$ and $\mu_s'$ uncertainties, determined from the phase and amplitude fits, range from 0.5% to 5% of the mean value.

Results of 674-nm FDPM measurements are shown for patient 1 in Figure 8. Raw data reveal clear differences in both phase (Figure 8*A*) and amplitude (Figure 8*B*) for normal and tumor sites. Solid lines are results of model-fits data demonstrating good agreement between measurements and the photon migration theoretical model. Only 10% of the actual data points is shown in each figure for clarity.

Optical properties calculated from each scan position are compared to mean values obtained from 11 discrete locations on the normal side. Figure 9*A* presents the ratio of absorption coefficients (tumor/normal) acquired in medial–lateral and superior–inferior scans at 674 nm.

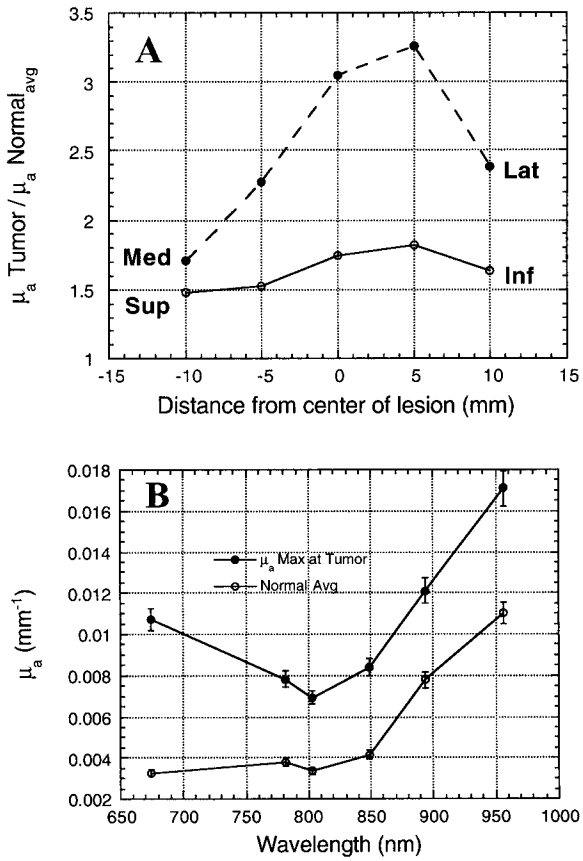


**Figure 9.** *(A) Ratio of absorption coefficients (tumor/normal) acquired in medial–lateral and superior–inferior scans at 674 nm for patient 1 (ductal carcinoma in situ, DCIS). Normal side represents average of 11 multiple site measurements. Contrast of approximately three-fold is observed for tumor vs. normal sites when the probe is placed 5 mm lateral of the estimated tumor center. (B) Wavelength dependence of optical properties acquired from the peak contrast location (5 mm lateral, medial–lateral axis) and symmetric location on normal side.*

Contrast of approximately three-fold is observed for tumor versus normal sites when the probe is placed just 5 mm lateral of the tumor center. A clearly discernable tumor shape is apparent in this horizontal scan direction. Reduced tumor/normal absorption contrast is observed in the superior–inferior scan, most probably due to differences in tumor orientation along this axis.

Wavelength-dependent optical properties acquired from the peak contrast location (5 mm lateral, medial–lateral axis) are displayed in Figure 9*B*. Absolute tumor $\mu_a$

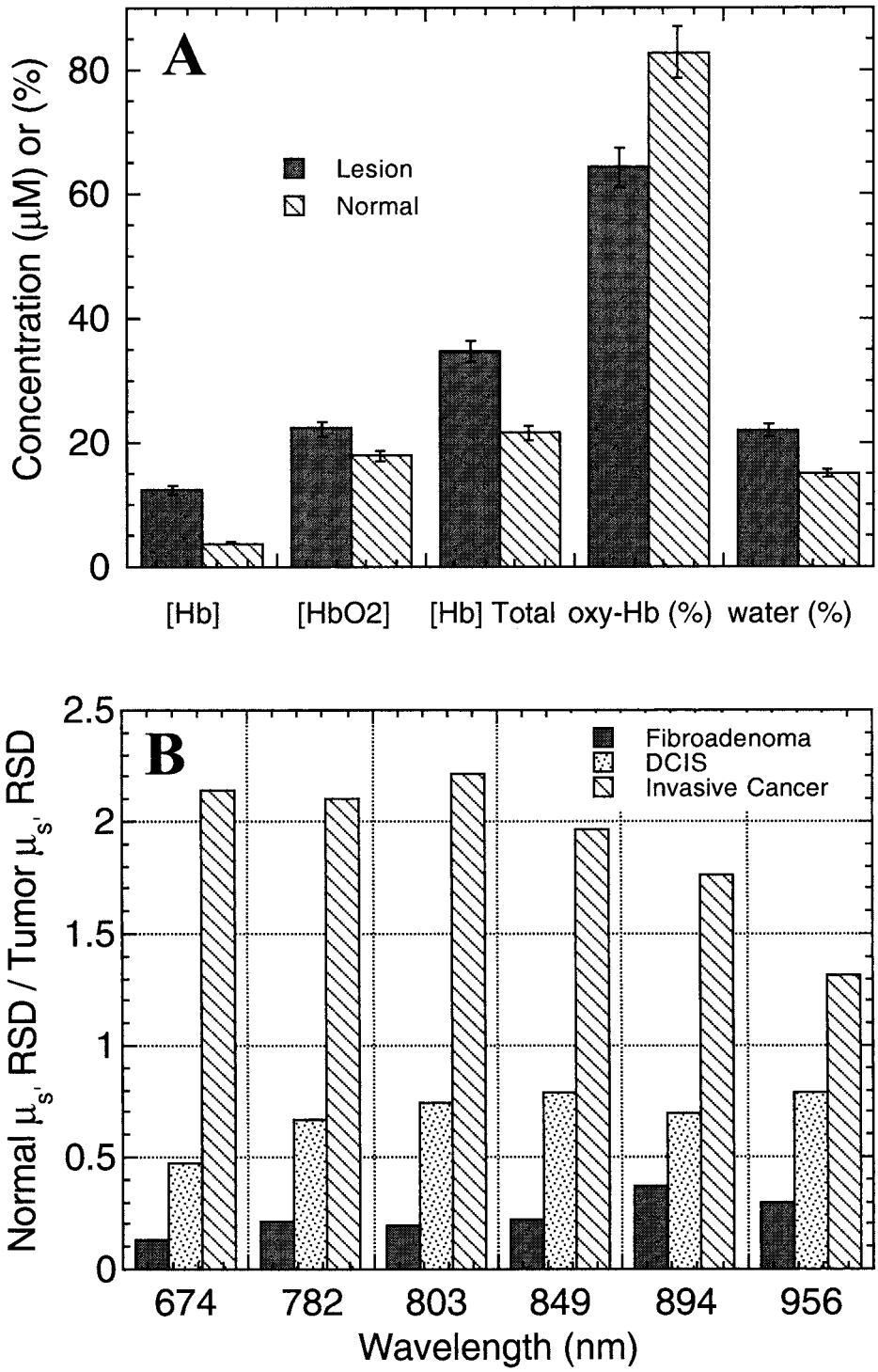


**Figure 10.** *(A) Hemoglobin concentration (μM) in deoxy- [Hb], oxy- [$HbO_2$], and total forms; %oxygen saturation (100× [$HbO_2$]/[Hb(tot)]), and water content (%) for normal and tumor breast, patient 1. Values calculated from wavelength dependence of absorption (Figure 9B). (B) The ratio of $\mu_s'$ RSD values for normal/tumor tissues at each measurement wavelength for patients 1 (DCIS), 2 (invasive ductal carcinoma), and 3 (benign fibroadenoma). RSD is determined from the mean and standard deviation of 11 measurements and nine discrete locations on normal and tumor sides. A RSD ratio of 1 implies that tumor and normal tissue have equivalent structural variation.*

values range from a minimum of about 0.007 $mm^{-1}$ at 803 nm to a maximum of 0.017 $mm^{-1}$ at 956 nm. Regardless of wavelength, tumor absorption is consistently on the order of 2- to 3.5-fold greater than normal tissue. This is due to the enhanced tumor versus normal blood supply (perfusion) and higher hemoglobin content. Tumor and normal tissue absorption spectra also have different shapes. The slope between 674 and 803 nm features is negative for tumor, positive for normal tissue. The significance of this is related to the increased contribution of de-oxyhemoglobin to light absorption in spectral regions that are shorter in wavelength than the ~800 nm isosbestic point (i.e., the point of equivalent absorption efficiency for both oxy- and deoxy-hemoglobin forms).

Physiologic differences between tumor and normal tissue are further amplified by calculations of water and blood content. The concentrations of water, deoxy-, oxy-, and total hemoglobin in DCIS and normal breast are determined from known extinction coefficients and Figure 9*B* absorption data. Results, shown in Figure 10*A*, clearly reveal elevated tumor levels for each physiological parameter. Total tumor hemoglobin ($[Hb(tot)] = [Hb] + [HbO_2]$) is 35 $\mu$M, nearly twice the 20 $\mu$M level typical of normal postmenopausal breast. Deoxy-hemoglobin ($[Hb]$) values of about 15 $\mu$M are roughly three-fold greater than normal. Together, these values can be used to determine percent oxygen saturation, $Y$, where $Y\% = 100 \times [HbO_2]/[Hb(tot)]$. In this case, $Y$(tumor) ~65% and $Y$(normal) ~80%. Differences are due to the oxygen extraction demands of rapidly proliferating, metabolically active tumor cells. The reduced $Y$ value is consistent with the measured elevation in hemoglobin at the tumor since both blood and oxygen are required to sustain tumor growth. Others have reported similar changes in tumor hemoglobin concentration and oxygen saturation using non-invasive photon migration techniques in the breast [46,47].

Tissue water concentration is also displayed in Figure 10*A*. It is difficult to confirm the accuracy of these values since they are based on pure water extinction coefficients (as opposed to protein-bound forms) at 25°C and our calculations do not take into account the contribution of fat to the 956 nm signal. Nevertheless, results fall within the 11.4% to 30.5% range given in the literature for percentage water in human fatty adipose tissue [48]. In addition, tumors develop high interstitial fluid pressure due to lack of lymphatic drainage. Thus, increased fluid retention, blood content, and cellularity are likely to be the cause of the slightly elevated tumor water percentage observed in this patient (20% vs. 15%).

Despite these clear biochemical differences, it is not yet known whether malignant tumors can be distinguished from benign lesions using this technology. In fact, it is our experience that both malignant and benign tumors generally display elevated hemoglobin and reduced $Y$% values. Although these observations are for a limited number of patients, it is likely that additional diagnostic specificity is required. This can be provided by examining spatial variations in the tissue-scattering parameter, $\mu_s'$. As illustrated schematically in Figure 8, normal well-differentiated tissue is composed of distinct structural/functional domains. The appearance of disease perturbs this intrinsic organization, resulting in a gradual loss of structural heterogeneity. Ultimately, the growth of an invasive tumor will lead to a chaotic, poorly differentiated environment.

The precise relationship between disease progression stage and photon migration-scattering signature is poorly understood. In order to explore this more carefully, we have mapped tumor optical properties from three patients with benign, malignant invasive, and malignant in situ breast disease. As described above, data are acquired from at least 11 measurements (nine discrete locations in 5 mm increments) using a $2 \times 2$ $cm^2$ scanning pattern on the breast surface. Absorption and scattering coefficients are computed and mean ± standard deviation (SD) values calculated for all measurements of normal and tumor-containing sites. The relative standard deviation (RSD) of optical properties obtained from tumor and normal sites is expressed in the usual manner, $RSD = 100 \times (SD/mean)$. Figure 10*B* shows the ratio of $\mu_s'$ RSD values for normal/tumor tissues at each measurement wavelength. A RSD ratio of 1 implies that tumor and normal tissue have equivalent structural variation. Interestingly, in the case of invasive cancer, the normal/tumor RSD is consistently greater than 1 for all wavelengths. This suggests greater scattering spatial heterogeneity in the well-differentiated normal tissue than in the lesion. These observations are consistent with the idea that disease progression leads to loss of differentiation, and that differentiation provides the fundamental origin for spatially varying scattering signals.

RSD ratios of about 0.5 and less are consistently observed with malignant DCIS and benign fibroadenomas. In the case of the fibroadenoma, this is likely due to enhanced structural variation (versus normal tissue) introduced by well-defined zones of dense collagen fiber synthesis and glandular shrinkage. DCIS appears to be midway between these two extremes, possibly due to the absence of invasion and general preservation/stimulation of extracellular matrix. These data further confirm the sensitivity of FDPM to the cell and matrix alterations seen in Figure 7. However, by measuring spatially varying properties, the perturbative effect tumors have on normal tissue architecture is detected with enhanced sensitivity.

## Conclusions

FDPM is a non-invasive optical technique that utilizes NIR light to monitor physiology in bulk tissues. Optical properties derived from FDPM measurements can be used to construct low-resolution functional maps and, consequently, provide a relatively low-cost adjunct to many conventional diagnostic tools. Substantial work remains to accurately describe heterogeneous tissues that vary in geometry, structure, and composition. Despite these limitations, several unique applications of photon migration

measurements are currently underway, particularly in solid tumor characterization. Preliminary studies show that unique breast tumor optical signatures are, in fact, detectable in human subjects. Changes in blood flow, oxygen consumption, and tissue structure (cellular and matrix) can be measured quantitatively. Most importantly, these signals appear to reflect fundamental physiological processes associated with malignancy, disease progression, age and menopausal status. Because many attributes related to the origin, progression, and therapeutic response of breast cancer are common to other types of tumors, we expect continued optical technology development will have a broad impact on optical diagnosis and therapy.

**Acknowledgements**

The authors wish to thank Andy Dunn and Joon You for assistance with Monte Carlo simulations.

## References

[1] Cutler M (1929). Transilluminating as an aid in the diagnosis of breast lesions. *Surg Gynecol Obstet* **48**, 721–728.

[2] Vastag B (1999). Shining light on breast tumors. *J Nat Cancer Inst* **91** (24), 2072–2073.

[3] Bonner RF, Nossal R, Havlin S, and Weiss GH (1987). Model for photon migration in turbid biological media. *J Opt Soc Am A* **4**, 423–432.

[4] Boulnois JL (1986). Photophysical processes in recent medical laser developments: a review. *Lasers Med Sci* **1**, 47–66.

[5] Svaasand L (1990). On the Physical Rationale of Photodynamic Therapy. In *Future Directions and Application in Photodynamic Therapy*. CJ Gomer (Ed.). SPIE Institute Series for Advanced Optical Technologies, IS6. pp. 233–248.

[6] Cheong WF, Prahl SA, and Welch AJ (1990). A review of the optical properties of biological tissues. *IEEE JQE* **26**, 2166–2185.

[7] Chance B, Leigh J, Miyake H, Smith D, Nioka S, Greenfield R, Finlander M, Kaufmann K, Levy W, Yound M, Cohen P, Yodshioka H, and Boretsky R (1988). Comparison of time-resolved and -unresolved measurements of deoxyhemoglobin in brain. *Proc Natl Acad Sci* **85**, 4971–4975.

[8] Delpy DT, Cope M, van de Zee P, Arridge S, Wray S, and Wyatt J (1988). Estimation of optical pathlength through tissue from direct time of flight measurement. *Phys Med Biol* **33**, 1433–1442.

[9] Wilson BC, Sevick EM, Patterson MS, and Chance B (1992). Time-dependent optical spectroscopy and imaging for biomedical applications. *Proc IEEE* **80**, 918–930.

[10] Cubeddu R, Pifferi A, Taroni P, Torricelli A, and Valentini G (1996). Experimental test of theoretical models for time-resolved reflectance. *Med Phys* **23** (9), 1625–1633.

[11] Zaccanti G, Bruscaglioni P, Ismaelli A, Carraresi L, Gurioli M, and Wei Q (1992). Transmission of a pulsed thin light beam through thick turbid media; experimental results. *Appl Opt* **31** (12), 2141–2147.

[12] Patterson MS, Chance B, and Wilson BC (1989). Time-resolved reflectance and transmittance for the non-invasive measurement of tissue optical properties. *Appl Opt* **28**, 2331–2336.

[13] Yoo KM, and Alfano RR (1990). Determination of the scattering and absorption lengths from the temporal profile of a backscattered pulse. *Opt Lett* **15**, 276–278.

[14] Singer JR, Grunbaum FA, Kohn P, and Zubelli JP (1990). Image reconstruction of the interior of bodies that diffuse radiation. *Science* **248**, 990–993.

[15] Barbour RL, Graber HL, Aronson R, and Lubowsky J (1991). Imaging of subsurface regions of random media by remote sensing. *Proc SPIE (Los Angeles)* **1431**, 192–203.

[16] Benaron D, and Stevenson D (1993). Optical time of flight and absorbance imaging of biologic media. *Science* **259**, 1463–1466.

[17] Ts'o DY, Frostig RD, Lieke EE, and Grinvald A (1990). Functional organization of primate visual cortex revealed by high resolution optical imaging. *Science* **249**, 417–420.

[18] Gratton E, Fantini S, Franceschini MA, Gratton G, and Fabini M (1997). Measurements of scattering and absorption changes in muscle and brain. *Philos Trans Biol Sci* **352**, 727–735.

[19] Sevick EM, Chance B, Leigh J, Nioka S, and Maris M (1991). Quantitation of time and frequency-resolved optical spectra for the determination of tissue oxygenation. *Anal Biochem* **195**, 330–351.

[20] Chance B, Nioka S, Kent J, McCully K, Fountain M, Greenfeld R, and Holtom G (1988). Time-resolved spectroscopy of hemoglobin and myoglobin in resting and ischemic muscle. *Anal Biochem* **174**, 698.

[21] Schmitt JM, and Zhou G-X (1992). Measurement of blood hematocrit by dual-wavelength near-IR photoplethysmography. In *Proc. SPIE 1641, Physiological Monitoring and Early Detection Diagnostic Methods.* TS Mang (Ed.). pp. 150–161.

[22] De Blasi RA, Fantini S, Franceschini MA, Ferrari M, and Gratton E (1995). Cerebral and muscle oxygen saturation measurement by a novel frequency-domain near-infrared spectrometer. *Med Biol Eng Commun* **33**, 228–230.

[23] Franceschini MA, Gratton E, and Fantini S (1999). Noninvasive optical method of measuring tissue and arterial saturation: an application to absolute pulse oximetry of the brain. *Opt Lett* **24** (12), 829–831.

[24] Patterson MS, Wilson BC, Feather JW, Burns DM, and Pushka W (1987). The measurement of dihematoporphyrin ether by reflectance spectrophotometry. *Photochem Photobiol* **46**, 337–343.

[25] Hornung R, Pham T, Keefe KA, Berns MW, Tadir Y, and Tromberg BJ (1999). Quantitative near-infrared spectroscopy of cervical dysplasia *in vivo*. *Hum Reprod* **14** (11), 2908–2916.

[26] Jacques SL, and Prahl SA (1987). Modeling optical and thermal distributions in tissue during laser irradiation. *Lasers Surg Med* **6**, 494–503.

[27] Furutsu K (1980). Diffusion equation derived from space–time transport equation. *J Opt Soc Am* **70**, 360.

[28] Patterson MS, Wilson BC, and Wyman DR (1991). The propagation of optical radiation in tissue: I. Models of radiation transport and their application. *Lasers Med Sci* **6**, 155–168.

[29] Jacques SL (1989). Time-resolved propagation of ultrashort laser pulses within turbid tissues. *Appl Opt* **28**, 2223–2229.

[30] Flock ST, Patterson MS, Wilson BC, and Wyman DR (1989). Monte Carlo modeling of light propagation in scattering tissues: I. Model prediction and comparison with diffusion theory. *IEEE Trans Biomed Eng* **36**, 1162–1168.

[31] Hasegawa Y, Yamada Y, Tamura M, and Nomura Y (1991). Monte Carlo simulation of light transmission through living tissues. *Appl Opt* **31**, 4515–4520.

[32] Ishimaru A (1989). Diffusion of light in urbid materials. *Appl Opt* **28**, 2210–2215.

[33] Dunn AK, Wallace VP, Coleno M, Berns MW, and Tromberg BJ Influence of optical properties on two-photon fluorescence imaging in turbid samples. *Appl Opt*, submitted.

[34] Fishkin J, and Gratton E (1993). Propagation of photon density waves in strongly scattering media containing an absorbing "semi-infinite" plane bounded by a straight edge. *J Opt Soc Am A* **10** (1), 127–140.

[35] Chance B, Cope M, Gratton E, Ramanujam N, and Tromberg B (1998). Phase measurement of light absorption and scatter in human tissues. *Rev Sci Instrum* **689**, 3457–3481.

[36] Haskell RC, Svaasand LO, Tsay T-T, Feng T-C, McAdams MS, and Tromberg BJ (1994). Boundary conditions for the diffusion equation in radiative transfer. *J Opt Soc Am A* **11**, 2727–2741.

[37] Madsen SJ, Anderson ER, Haskell RC, and Tromberg BJ (1994). A portable, high-bandwidth frequency-domain photon migration instrument for tissue spectroscopy. *Opt Lett* **19**, 1934–1936.

[38] Bigio IJ, and Mourant JR (1997). Ultraviolet and visible spectroscopies for tissue diagnostics: fluorescence spectroscopy and elastic-scattering spectroscopy. *Phys Med Biol* **42**, 803–814.

[39] Perelmand LT, Backman V, Wallace M, Zonios G, Manoharan R, Nusrat A, Shields S, Seiler M, Lima C, Hamano T, Itzkan I, Van Dam J, Crawford JM, and Feld MS (1998). Observation of periodic fine structure in reflectance from biological tissue: a new technique for measuring nuclear size distribution. *Phys Rev Lett* **80** (3), 627–630.

[40] Boas DA, O'Leary MA, Chance B, and Yodh AG (1997). Detection and characterization of optical inhomegeneities with diffuse photon density waves: a signal-to-noise analysis. *Appl Opt* **36**, 75–92.

[41] Fishkin JB, Coquoz O, Anderson EA, Brenner M, and Tromberg BJ (1997). Frequency-domain photon migration measurements of normal and malignant tissue optical properties in a human subject. *Appl Opt* **36**, 10–20.

[42] Thompsen S, and Tatman D (1998). Physiological and pathological

factors of human breast disease that can influence optical diagnostics. *Ann NY Acad Sci* **838**, 171–193.

[43] Suzuki K, Yamashita Y, Ohta K, Kaneko M, Yoshida M, and Chance B (1996). Quantitative measurement of optical parameters in normal breasts using time-resolved spectroscopy: *in vivo* results of 30 Japanese women. *J Biomed Opt* **1** (3), 330–334.

[44] Quaresima V, Matcher SJ, and Ferrari M (1998). Identification of intrinsic optical contrast for near-infrared mammography. *Photochem Photobiol* **67** (1), 4–14.

[45] Tromberg BJ, Coquoz O, Fishkin JB, Pham T, Anderson ER, Butler J, Cahn M, Gross JD, Venugopalan V, and Pham D (1997). Non-invasive measurements of breast tissue optical properties using frequency-domain photon migration. *Philos Trans R Soc London B* **352**, 661–668.

[46] Fantini S, Walker SA, Franceschini MA, Moesta KT, Schlag PM, Kaschke M, and Gratton E (1998). Assessment of the size, position, and optical properties of breast tumors *in vivo* by non-invasive optical methods. *Appl Opt* **37**, 1982–1989.

[47] McBride TO, Pogue B, Gerety ED, Poplack SB, Osterberg UL, and Paulsen KD (1999). Spectroscopic diffuse optical tomography for the quantitative assessment of hemoglobin concentration and oxygen saturation in breast tissue. *Appl Opt* **38** (25), 5480–5491.

[48] Duck FA (1990). *Physical Properties of Tissue*. London, Academic Press. pp. 320–328.